

NGC 2401: a template of the young population of the Norma–Cygnus arm in the Third Galactic Quadrant[★]

G. Baume,^{1,2†} A. Moitinho,³ R. A. Vázquez,¹ G. Solivella,¹ G. Carraro^{2,4,5}
and S. Villanova²

¹Facultad de Ciencias Astronómicas y Geofísicas de la UNLP, IALP-CONICET, Paseo del Bosque s/n, La Plata, Argentina

²Dipartimento di Astronomia, Università di Padova, Vicolo Osservatorio 2, I-35122 Padova, Italy

³CAAUL, Observatório Astronómico de Lisboa, Tapada da Ajuda, 1349-018 Lisboa, Portugal

⁴Astronomy Department, Yale University, PO Box 208101, New Haven, CT 06520-8101 USA

⁵Departamento de Astronomía, Universidad de Chile, Casilla 36-D, Santiago, Chile

Accepted 2005 December 9. Received 2005 December 9; in original form 2005 July 26

ABSTRACT

Based on a deep optical CCD $[UBV(RI)_C]$ photometric survey and on the Two-Micron All Sky Survey (2MASS) data, we derived the main parameters of the open cluster NGC 2401. We found that this cluster is placed at 6.3 ± 0.5 kpc ($V_O - M_V = 14.0 \pm 0.2$) from the Sun and is 25 Myr old, which allows us to identify NGC 2401 as a member of the young population belonging to the innermost side of the extension of the Norma–Cygnus spiral arm in the Third Galactic Quadrant. A spectroscopic study of the emission star LSS 440 that lies in the cluster area revealed that it is a B0Ve star; however, we could not confirm that it is a cluster member. We also constructed the cluster luminosity function (LF) down to $V \sim 22$ and the cluster initial mass function (IMF) for all stars with masses above $M \sim 1\text{--}2 M_\odot$. It was found that the slope of the cluster IMF is $x \approx 1.8 \pm 0.2$. The presence of a probable pre-main-sequence (PMS) star population associated with the cluster is weakly revealed.

Key words: stars: emission-line, Be – stars: imaging – stars: individual: LSS 440 – stars: luminosity function, mass function – open clusters and associations: individual: NGC 2401 – Galaxy: structure.

1 INTRODUCTION

The open cluster NGC 2401 (= OCL 588 = C0727-138) is an almost unstudied compact grouping of faint stars, but for identification and eye estimates of its angular size and richness. According to the Lyngå (1987) classification, this object is a Trumpler class II 3 p with an ~ 2 -arcmin diameter, which is the same diameter listed in Dias et al. (2002). A recent photometric study on this area carried out by Sujatha, Babu & Ananthamurphy (2004) yielded an intriguing result where a relatively far cluster (located at a distance of about 3.1 kpc) shows only a colour excess $E(B - V) = 0$. This fact alone deserves our total attention. Moreover, because NGC 2401 is placed in the Puppis region ($l = 229^\circ 67'$; $b = +1^\circ 85'$) in the poorly studied Third Quadrant of the Galaxy, the determination of its basic parameters will contribute, together with other cluster studies in the region, to describe more precisely the spiral structure and the star formation history in this part of the Galaxy. This region contains several distant clusters through which information on the kinemat-

ics and evolutionary status of the stellar population in the outermost parts of the Galactic disc can be obtained. In fact, because the detection of the Canis Major overdensity (see e.g. Martin et al. 2004 and Momany et al. 2004 for more details), there is a growing interest to get a better description of the stellar population in this region of the Galaxy.

Preliminary results of NGC 2401 can be found in a CCD $UBV RI$ photometric data base by Moitinho (2001, 2002) containing brief information for 30 open clusters in the Galactic longitude range $217^\circ < l < 260^\circ$. Also recently, Giorgi et al. (2002, 2005), Carraro & Munari (2004), Baume et al. (2004), Carraro et al. (2005a) and Moitinho et al. (2006) published studies of a series of largely overlooked open clusters in the same Galactic region.

In this paper, we present a detailed study of the membership, reddening, distance and age of NGC 2401. They were derived together with the luminosity function (LF) and initial mass function (IMF), two distributions that are fundamental tools for understanding the star formation mechanisms and related astrophysical problems. We also present the first spectrum analysis of the peculiar emission star LSS 440 located in the cluster field and try to clarify the possible connection of both objects.

In the next section, we introduce the observational material. Section 3 is aimed at analysing the photometric diagrams and to

[★]Based on observations collected at CTIO and the ESO and CASLEO; data are only available in electronic form at the Centre de Données astronomiques de Strasbourg (CDS).

†E-mail: gbaume@fcaglp.unlp.edu.ar

determine memberships. In Section 4, we discuss the LSS 440 main properties; in Section 5, we construct and discuss both the LF and IMF. In Section 6, we studied the possible presence of pre-main-sequence (PMS) stars and, finally, in Sections 7 and 8, we discuss the main findings of this investigation and present the conclusions, respectively.

2 DATA SET

2.1 Optical photometric data

CCD $UBV(RI)_C$ images of NGC 2401 were acquired with the Cerro Tololo Inter-American Observatory (CTIO) 0.9-m telescope during an observing run in 1998 January. Observations, reductions, error analysis, and comparison with other photometries were thoroughly described in Moitinho (2001). Additionally, further CCD $V(I)_C$ images were obtained for this object at the European Southern Observatory (ESO; La Silla) with the ESO Multi-Mode Instrument (EMMI) camera mounted on the New Technology Telescope (NTT) during the night of 2002 December 9. Typical seeing was about 1 arcsec. The camera has a mosaic of two 2048×4096 pixel CCDs, which samples a $9.9 \text{ arcmin} \times 9.1 \text{ arcmin}$ field. The images were binned 2×2 , resulting in a scale of $0.332 \text{ arcsec pixel}^{-1}$. Details on the reductions of these kind of data were given in Baume et al. (2004). The fields covered by CTIO and ESO observations are shown in Fig. 1.

Combining both data sets required a detailed comparison of their plate scales and photometric scales. While matching the X, Y pixel coordinates from both sets, we noticed that no one-to-one correspondence could be satisfactorily achieved through a simple linear transformation. Indeed, the residuals of the transformation displayed a jump in the middle of the NTT X -axis. This is likely due to the junction between the two CCDs that compose the EMMI camera. Once taking this effect into account, the NTT coordinates were transformed without trouble to the system of the CTIO X - Y positions, and sources from both sets were cross-identified. The rms residuals

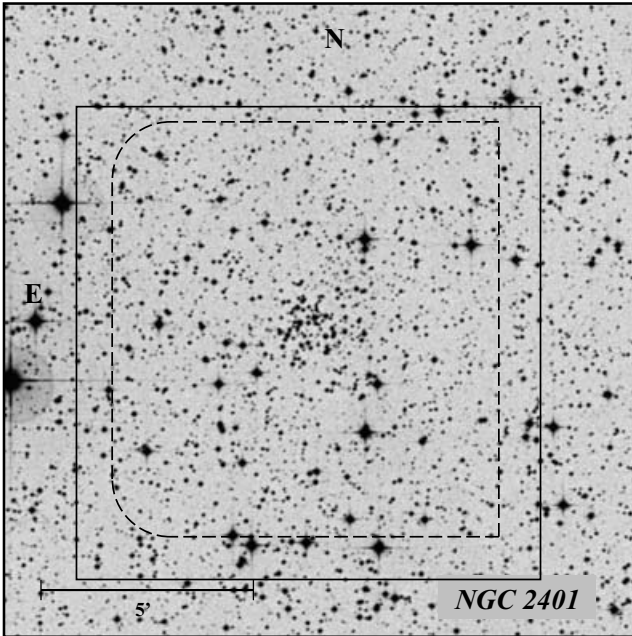


Figure 1. Second generation Digitized Sky Survey (DSS-2), red filter image of the field of NGC 2401. The areas covered by the CTIO and ESO observations are indicated by solid and dashed lines, respectively.

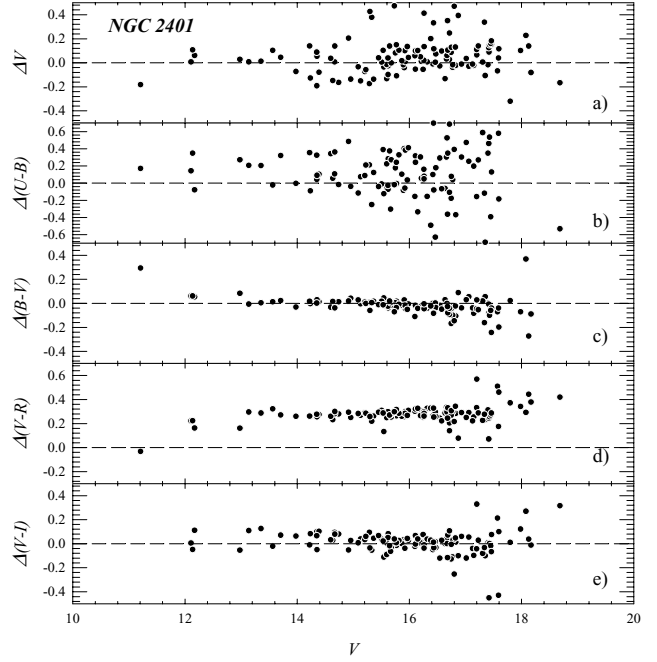


Figure 2. Comparison of our photometry with Sujatha et al. (2004) in the sense ‘Our data – Their data’ (115 stars). Mean differences and their standard deviations (sd) were: $\Delta V = +0.05 \pm 0.14(\text{sd})$, $\Delta(B - V) = -0.02 \pm 0.10(\text{sd})$, $\Delta(U - B) = +0.06 \pm 0.39(\text{sd})$, $\Delta(V - R) = +0.28 \pm 0.07(\text{sd})$ and $\Delta(V - I) = +0.00 \pm 0.11(\text{sd})$.

of the transformations were around 0.15 CTIO pixels (1 CTIO pixel ≈ 0.39 arcsec). The NTT VI measurements were then tied to the CTIO photometry through linear transformations of the form $V_{\text{CTIO}} - V_{\text{NTT}} = \alpha_0 + \alpha_1(V - I)_{\text{NTT}}$; $(V - I)_{\text{CTIO}} = \beta_0 + \beta_1(V - I)_{\text{NTT}}$, using stars with estimated errors less than 0.015 mag, which essentially corresponds $V_{\text{CTIO}} < 18$ mag. The rms of the photometric transformations were ≈ 0.02 mag. Both photometries were then combined by averaging the measurements weighted by their errors. The errors in the CTIO magnitudes are described in Moitinho (2001) and are taken to be the dispersion of the measurements when repeated observations were available, or the errors output by ALLSTAR in the case of single measurements. For the NTT magnitudes, the adopted errors were those given by ALLSTAR.

We also cross-correlated our data with the ones given by Sujatha et al. (2004) to compare both photometric sets. Fig. 2 shows a relatively good agreement in the mean values for V magnitudes and $B - V$ and $V - I$ colours, though the V magnitude spread is quite significant. In addition, there is a noticeable shift between both data sources when $U - B$ and $V - R$ colours are compared. In particular, the spread in $U - B$ is simply huge. These differences could be explained by the different spatial resolution of each observation set (some crowded areas in the Sujatha et al. data were resolved by us), zero-point differences in their $U - B$ and $V - R$ measures probably caused by poor atmospheric conditions in the Sujatha et al. observing run and the rather poor quality of their U filter. This way, the strange colour excess value $E(B - V) = 0$ computed by them can be explained. It is worth mentioning that our data produce coherent fitting solutions over all the photometric diagrams (see Section 3 and Fig. 6, below). On the other hand, our photometric data are based on a more general and homogeneous data set (Moitinho 2001), which is in agreement with previous studies (when the comparison was possible).

Table 1. Photometric catalogue of the NGC 2401 region.

ID	X (arcsec)	Y (arcsec)	α_{2000}	δ_{2000}	V	B - V	U - B	V - R	V - I	K	J - K	H - K	Comments
1	81.5	-164.7	07 ^h 29 ^m 19 ^s .6	-14°00'38".7	10.181	0.033	-0.463	-	-	10.230	-0.086	-0.010	- -
2	82.2	109.6	07 ^h 29 ^m 19 ^s .6	-13°56'04".4	11.208	1.243	0.991	0.638	-	8.284	0.715	0.223	CA nm
3	-108.3	-310.5	07 ^h 29 ^m 32 ^s .6	-14°03'04".5	11.316	0.664	0.000	0.290	-	9.856	0.303	0.113	- -
4	-81.4	-324.7	07 ^h 29 ^m 30 ^s .8	-14°03'18".7	11.347	1.849	1.904	0.984	-	6.729	1.101	0.328	- -
5	233.9	100.6	07 ^h 29 ^m 09 ^s .1	-13°56'13".4	11.422	1.437	1.163	0.748	1.449	7.963	0.844	0.249	CF -
:	:	:	:	:	:	:	:	:	:	:	:	:	:
3259	122.6	258.2	07 ^h 29 ^m 16 ^s .8	-13°53'35".8	23.666	-	-	-	2.569	-	-	-	- -
3260	-224.9	-99.9	07 ^h 29 ^m 40 ^s .7	-13°59'33".9	23.700	-	-	-	2.853	-	-	-	CF -
3261	97.4	198.2	07 ^h 29 ^m 18 ^s .5	-13°54'35".8	23.848	-	-	-	3.211	-	-	-	- -

A full version of this table including photometric errors is available in an electronic format at the CDS, and in the online version of this article on Synergy. Comments columns indicate: stars located in the ‘cluster area’ (CA) or in the ‘comparison field’ (CF; see Fig. 7 and Section 3.2); membership assignments (nm means non-member stars; see also Section 3.2).

2.2 Spectroscopic data

Spectral data for the star LSS 440 ($\alpha_{2000} = 07^{\text{h}}29^{\text{m}}30^{\text{s}}.1$, $\delta_{2000} = -13^{\circ}59'13''$) were obtained with the 215-cm telescope of CASLEO (Complejo Astronómico el Leoncito, Argentina) during the nights of 2004 December 6, 7 and 9. Observations were carried out with a REOSC-DS Cassegrain spectrograph equipped with a Tek 1024 × 1024 detector. The grating was successively centred at 7°15', 8°30' and 11°30' (on different nights) to get a full spectral range coverage from 3400 to 6750 Å in wavelength. The dispersion was 2.5 Å/pixel⁻¹ (resolution ≈ 1800). Two 30 min exposure time spectra were taken in each grating position to remove undesirable events such as cosmic rays and to improve the signal-to-noise ratio of the final spectrum. Comparison lamp (HeNeAr) spectra were acquired between each pair of exposures. Spectra were reduced using IRAF¹ routines like IMRED, CCDPROC, TWDSPEC and ONEDSPEC using the typical procedure.

2.3 Infrared data and astrometry

Available catalogues, such as the Two-Micron All Sky Survey (2MASS), are of fundamental importance to perform a more complete analysis of any sky region. Using the CCD X–Y positions of our data, we computed their equatorial coordinates. First of all, a matched list of X–Y and RA, Dec. was built by visually identifying about 20–30 Tycho-2 (Høg et al. 2000) and 2MASS stars in each cluster field. The stars in the list were used to obtain transformation equations to get equatorial coordinates for all our measured stars. In a second step, we use a computer routine to cross-identify all our sources in common with the same catalogues by matching the equatorial coordinates to the catalogued ones. The rms of the residuals were ~0.15 arcsec, which is about the astrometric precision of the 2MASS catalogue (~0.12 arcsec), as expected because most of the coordinates were retrieved from this catalogue.

This procedure allowed to build a photometric *UBVRIJHK* catalogue that constitutes the main observational data base used in this study. The catalogue is presented in Table 1, which includes our X–Y positions (in arcsec, see Fig. 7, below), equatorial coordinates (epoch 2000.0), optical and infrared photometry.

¹ IRAF is distributed by the National Optical Astronomy Observatories (NOAO), which are operated by the Association of Universities for Research in Astronomy, Inc. (AURA), under cooperative agreement with the National Science Foundation (NSF).

3 ANALYSIS

3.1 Cluster centre and size

As a first step, we estimated the position of the cluster centre. This procedure was performed by a combination of a visual inspection of the second generation Digitized Sky Survey (DSS-2) plates and the method given by Moitinho et al. (1997). In this later case, the surface stellar distribution was convolved with a kernel and the centre is adopted as the point of maximum density. In this case, a 100 × 100 CTIO pixel (≈ 0.66 arcmin × 0.66 arcmin) Gaussian kernel was used to smooth out the details of the spatial distribution and give a precise idea of the centre position. Fig. 3 illustrates the method. The derived centre was $\alpha_{2000} = 07^{\text{h}}29^{\text{m}}25^{\text{s}}.2$, $\delta_{2000} = -13^{\circ}57'54''$, nearby to the one given by Dias et al. (2002) or by the SIMBAD data base.

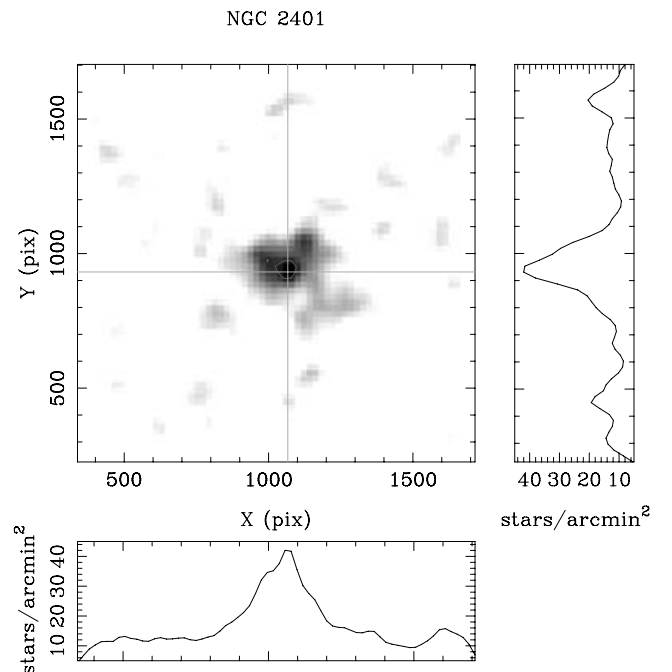


Figure 3. First approximation to the centre determination for NGC 2401. Top left: density map of the selected stars in the field. Top right: Y cut through the density maximum. Bottom: X cut through the density maximum.

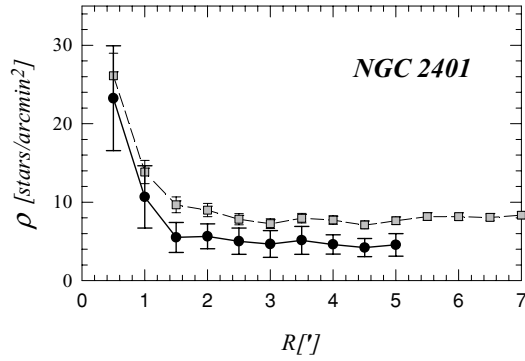


Figure 4. Radial density profiles for NGC 2401. Filled circles: CCD data. Grey squares: 2MASS data. Poisson error bars (1σ) are also shown.

The second step was to compute the cluster radial density profile by counting stars in a number of successive rings, 0.5 arcmin wide, and dividing the counts by the area of the corresponding ring. We applied this method to both the optical and the 2MASS infrared data. The respective radial density profiles are shown in Fig. 4. We appreciate a well-shaped radial stellar density profile for the cluster with an important central concentration up to ~ 1.5 arcmin, but we adopted a radius of $R = 2.5$ arcmin because, at this value, the stellar density reaches the (residual) field density. Our adopted value is a bit larger than the diameter of about 2 arcmin given by Lyngå (1987) and Dias et al. (2002). It seems that these works refer to the object size as only the very central part of the cluster. On the other hand, the radius we computed here is generous enough to include cluster stars (mainly faint ones) that could be placed a bit far from the cluster centre. In any case, our data completely covers the cluster together with an important part of its surrounding field.

3.2 Optical data and cluster membership

Information about proper motions and radial velocities for the stars in the area of NGC 2401 is scarce. The Second US Naval

Observatory CCD Astrograph Catalog (Zacharias et al. 2004) provides proper motion data for some stars in these area down to a magnitude about $V = 16$ that could help to perform a membership assignment. However, uncertainties of these measurements (~ 10 mas yr^{-1}) avoid using proper motions in a efficient way. Therefore, the only way to obtain a reliable membership assignment is by analysing the individual position of the stars onto several photometric diagrams (e.g. Baume et al. 2003, 2004).

The optical two-colour diagrams (TCDs) and colour-magnitude diagrams (CMDs) of NGC 2401 are shown in Figs 5 and 6, respectively. The TCDs of Fig. 5 and the CMDs of Figs 6(a), (b) (d) and (e) include all the stars inside the adopted radius for the cluster (see Section 3.1). For reference purposes, we adopted a comparison field (CF) defined by the short-dashed lines in the finding chart of Fig. 7. This CF was chosen in such a way that its area equals that corresponding to the cluster and it was also totally covered by the NTT observations. The CMDs of the CF are shown in Figs 6(c) and (f).

Different CMDs show different limiting V magnitudes going from ~ 19 in $U - B$ to ~ 23 in $V - I$ due to the dissimilar wavelength sensitivity of the detectors, on one side, and also because we combined data from two sources (see Section 2.1), on the other. Naturally, deep $V - I$ data came from the NTT.

All the diagrams confirm that NGC 2401 presents a very sharp, clear and blue main sequence (MS) above $V \sim 17-17.5$. For membership assignments, individual positions down to the magnitude limit were examined in all the photometric diagrams using the procedure described in Baume et al. (2004). This is as follows.

- (i) If stars brighter than $V \sim 16.5$ have coherent locations in all the TCDs and CMDs along the MS, they were adopted as likely members (lm). We shall discuss below the case of LSS 440 (see Section 4).
- (ii) Dimmer stars with magnitudes in the range $V \sim 16.5-17.5$ in the same conditions were considered only as probable members (pm).

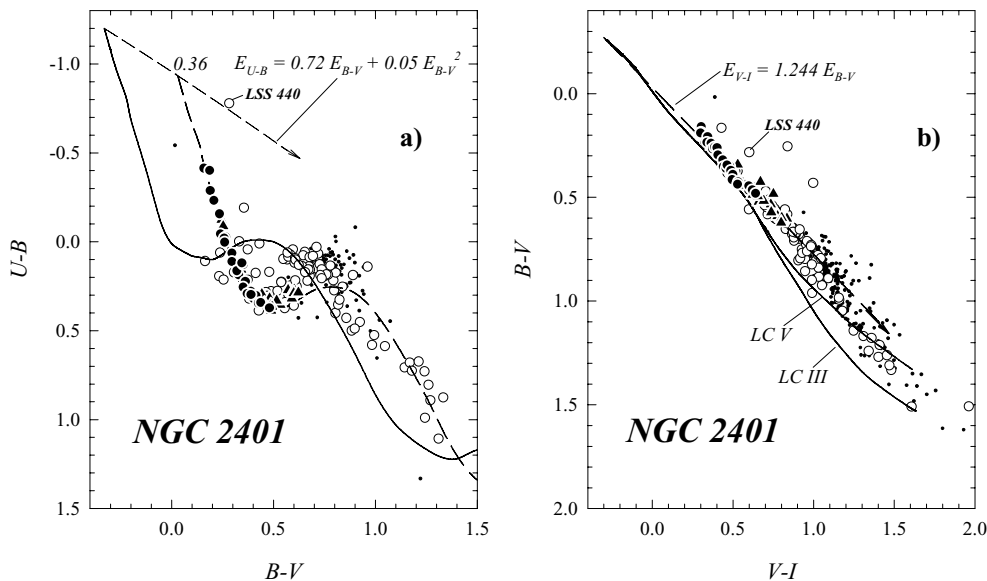


Figure 5. Optical TCDs of stars located inside the adopted radius of NGC 2401 (a) $U - B$ versus $B - V$ diagram. The symbols have the following meaning: black circles are adopted likely member stars (lm), black triangles are probable member stars (pm), white circles are non-member stars (nm) and dots are stars without any membership assignment. The solid line is the Schmidt-Kaler (1982) ZAMS, whereas the dashed one is the same ZAMS, but shifted by the adopted colour excess (see Section 3.3). The dashed arrow indicates the normal reddening path. (b) $B - V$ versus $V - I$ diagram. Symbols and lines have a similar meaning to those in panel (a).

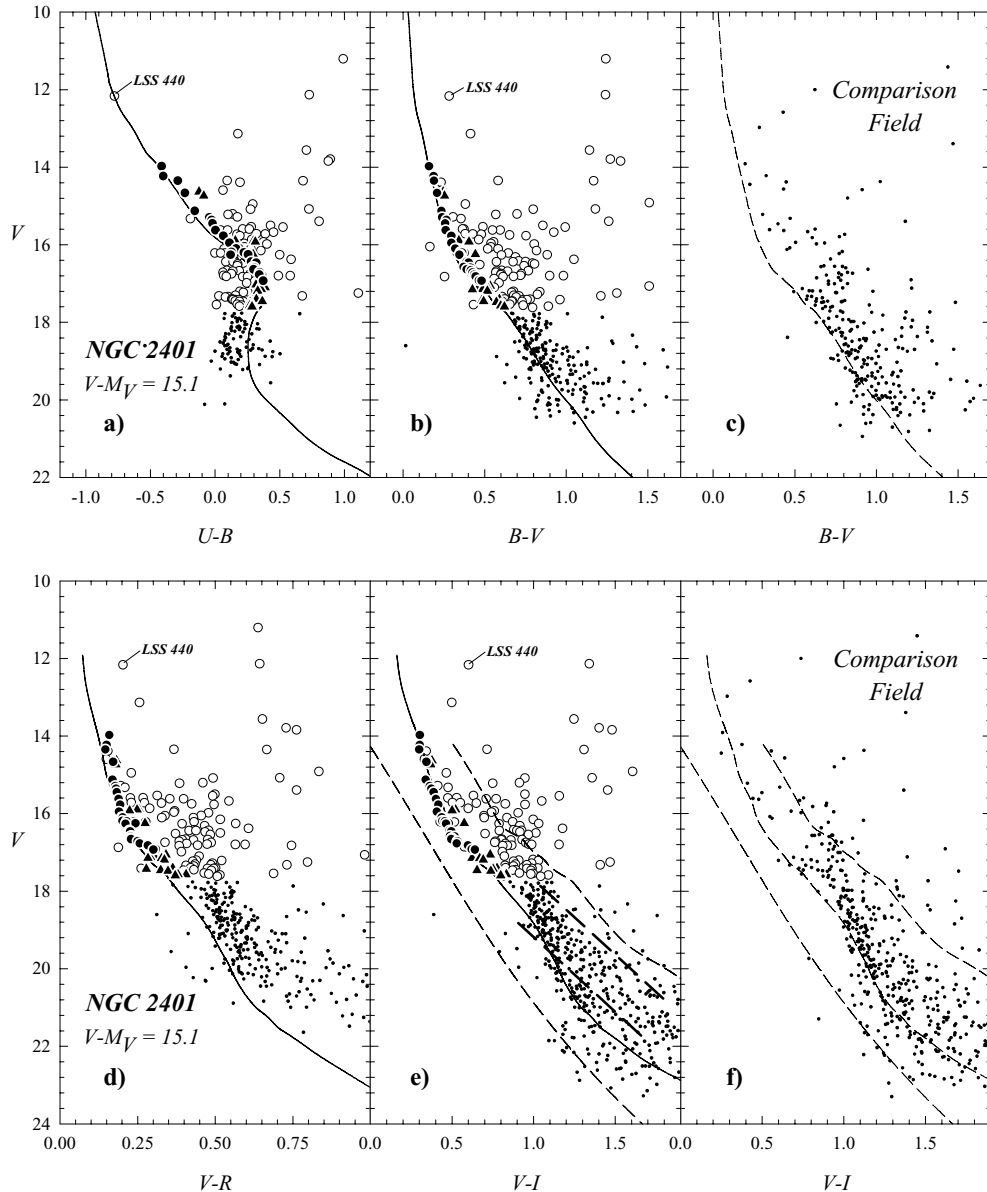


Figure 6. Optical CMDs of stars located inside the adopted radius of NGC 2401 (‘cluster area’, panels a, b, d and e) and in the adopted CF (panels c and f). Symbols have the same meaning as in Fig. 5. The solid lines are the Schmidt-Kaler (1982) and Cousins (1978a,b) empirical ZAMS and MS respectively, corrected for the effects of reddening and distance. The adopted apparent distance modulus is $V - M_V = 15.1$ ($V - M_V = V_0 - M_V + 3.1E(B - V)$; see Section 3.3). Dashed lines shown on the CF diagrams have the same meaning as the curves in the other panels: ZAMS, MS and the adopted envelopes used to compute the LF (see Section 5). See Section 6 for the meaning of long-dashed straight lines on panel (e).

(iii) If some stars are brighter than $V \sim 16.5$, well placed onto the TCDs of Fig. 5 but located a bit over the zero-age main-sequence (ZAMS) on Fig. 6, they were still considered as pm because their magnitude offsets could be due to a probable binarity effect. This was undoubtedly the case for stars nos 66 and 75, which, unlike likely members, appeared above the MS (~ 0.5 mag).

(iv) Finally, the number of likely and probable member stars in each magnitude bin must keep a reasonable agreement with the counts that were obtained when CF stars were adequately subtracted from the ‘cluster area’ (see Section 5).

At fainter magnitudes, contamination by field stars becomes severe, preventing an easy identification of faint cluster members. Anyway, it was still possible to determine the number of probable faint cluster members in a statistical way (see Sections 5 and 6).

3.3 Cluster parameters

3.3.1 Optical data

This region of the Third Galactic Quadrant is characterized by a reddening slope and a ratio of the total to selective absorption [$R = A_V/E(B - V)$] that can be considered normal (Moitinho 2001). Because the picture presented in the $B - V$ versus $V - I$ diagram in Fig. 5(b) agrees with this concept, we adopted standard ratios $E(U - B)/E(B - V) = 0.72 + 0.05 E(B - V)$ and $E(V - I)/E(B - V) = 1.244$ (Dean, Warren & Cousins 1978), which implies $R = 3.1$, to shift the Schmidt-Kaler (1982) ZAMS, the intrinsic lines from Cousins (1978a), Cousins (1978b) and the Girardi et al. (2000) isochrones in the TCDs and CMDs. By restricting to lm and pm stars, we found mean excess values and standard deviations

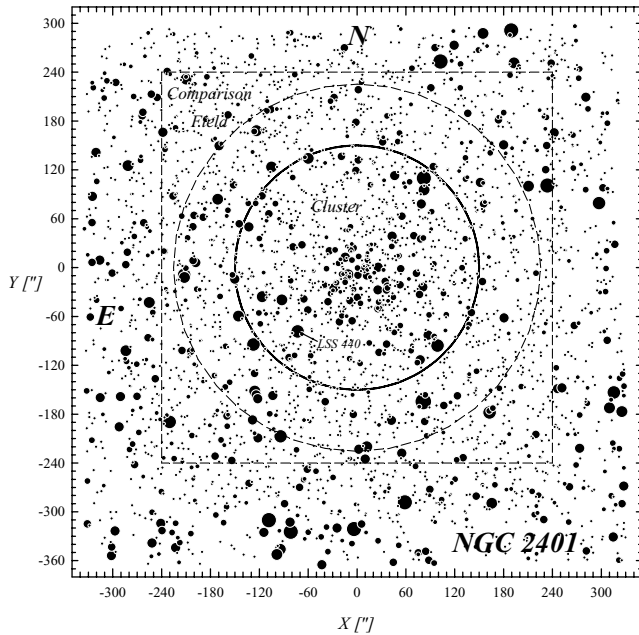


Figure 7. Finding chart of the observed region in NGC 2401 (V filter). The black solid circles, 2.5 arcmin in radius, indicate the adopted angular size for the cluster (see Section 3.1 and Fig. 4). The short-dashed lines indicate the area adopted as a comparison field (CF). For a coordinate reference, the $X = 0, Y = 0$ values correspond to the cluster centre coordinates $\alpha_{2000} = 07^{\text{h}}29^{\text{m}}25^{\text{s}}.2$, $\delta_{2000} = -13^{\circ}57'54''$ and all X - Y are expressed in arcseconds.

$E(B - V) = 0.36 \pm 0.01$ and $E(U - B) = 0.27 \pm 0.01$. As for the cluster distance modulus, we found $V - M_V = 15.1 \pm 0.2$ (error from eye inspection) by the fitting method. This distance modulus combined with a mean visual absorption $A_V = 1.12$ places NGC 2401 at 6.3 ± 0.5 kpc from the Sun.

The age of the cluster was derived superposing the isochrones of Girardi et al. (2000), computed with mass loss and overshooting (see Fig. 8) and solar metallicity, and looking for those ones that produce the best fit over the stars along the upper MS. This method yields that NGC 2401 is about 20 ± 5 Myr old. Another age indicator comes from the inferred earliest spectral type at the upper MS of the cluster. In NGC 2401, the earliest MS star may have a spectral type B3 and, according to the calibration given by Meynet, Mermilliod & Maeder (1993), the corresponding age is about 30 Myr. Therefore, we adopted 25 ± 5 Myr as a good estimation for NGC 2401 age.

3.3.2 Infrared data

As a control of the optical findings, we built up the CMDs indicated in Fig. 9 using 2MASS data (see Section 2.3). If we only consider the infrared colours (Fig. 9a), the data spread of 1m and pm stars is very significant though their mean values approximately follow the MS position given by Koornneef (1983). It is obvious that this spread is due to the infrared magnitude errors in the 2MASS catalogue at the level of $K \approx 14$ –15, as it is strongly reduced when combined with optical data to obtain the $V - K$ index (Fig. 9b). So, the distance modulus fit in the infrared diagrams turns out to be quite acceptable; in addition, infrared diagrams independently confirm that the reddening law is normal as suggested by the optical TCDs of Fig. 5.

As a final note, the infrared CMD of the CF (see Section 3.2) that is shown in Fig. 9(c) confirms that the region around the MS has almost no stars reinforcing the real nature of the cluster.

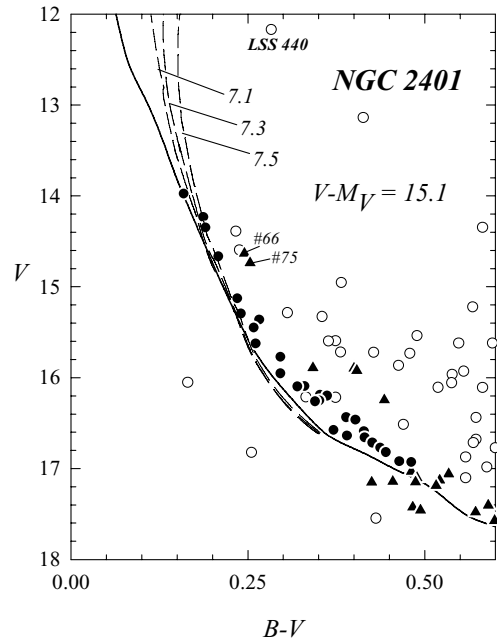


Figure 8. V versus $B - V$ CMD showing the isochrones (dashed lines) from Girardi et al. (2000) and the Schmidt-Kaler (1982) ZAMS (solid line) corrected for the effects of reddening and distance (see Section 3.3). Symbols have the same meaning as in Fig. 5. The numbers indicate $\log(\text{age})$.

4 THE BE-TYPE STAR LSS 440

A singular object in the field of NGC 2401 is the bright star no. 14 located at 1.8 arcmin south-east from the cluster centre. This star was identified early as LSS 440 by Stephenson & Sanduleak (1971) who informed that it is an OB-type star with the Balmer continuum in emission (in an exceptionally pronounced way) and the $H\alpha$ line in emission too according to an independent $H\alpha$ plate. To classify this star, a series of spectra were obtained covering the spectral range 3400–6750 Å (see Section 2.2). The LSS 440 spectrum is shown in Fig. 10 together with a detail of the most relevant features. This star shows the $H\alpha$ line in strong emission, together with $H\beta$ and $H\gamma$ lines in clear core emission and $H\delta$ only in a weak way. The Fe II 27, 37, 38, 42, 48, 49 and S II 19, 26 multiplets also appear in emission. The Balmer continuum is in emission too, but not as strong as Stephenson & Sanduleak (1971) claimed. The $H\alpha$ equivalent width is ~ 76 Å and the rotation velocity is near $v \sin i \sim 270$ –300 km s $^{-1}$ from He I lines 4471 and 4026.

The spectral classification of LSS 440 was performed using the Barbier–Chalonge–Divan (BCD) spectrophotometric system (see Barbier & Chalonge 1941, Chalonge & Divan 1952, Chalonge & Divan 1973 and Cidale, Zorec & Tringaniello 2001 for the description of the method). Briefly, the method is based on the study of the Balmer discontinuity, which is independent on interstellar and circumstellar extinctions. Using the obtained BCD parameters $\lambda_1 = 59.7$ Å, $D = 0.078$ dex and calibration tables given by Zorec (1986), we classified this star as B0Ve. The early type and the presence of emission Fe II lines could indicate LSS 440 as a member of Group I according to the classification scheme proposed by Jaschek et al. (1980).

The models given by Zorec et al. (2002) can be used to get the average photospheric properties for this star as well: $M_V = -3.6 \pm 0.5$, $T_{\text{eff}} = 30\,000 \pm 1000$ K, $\log g = 4.0 \pm 0.1$ and $M_{\text{bol}} = -6.5 \pm 0.2$. Combining with the Girardi et al. (2000) evolutionary models

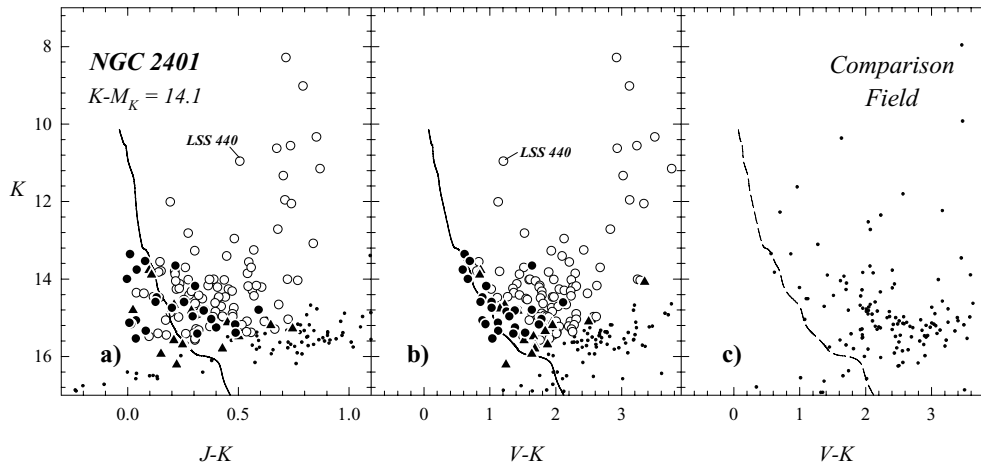


Figure 9. Infrared CMDs of stars located inside the adopted radius of NGC 2401 (panels a and b) and in the adopted comparison field (panel c). Symbols have the same meaning as in Fig. 5. The solid lines are the Koornneef (1983) empirical MS, corrected for the effects of reddening and distance [$K - M_K = 14.1 = V_0 - M_V + (3.1 - 2.78)E(B - V)$; see Section 3.3]. Dashed line shown on the comparison field has the same meaning as the curves in the other panels.

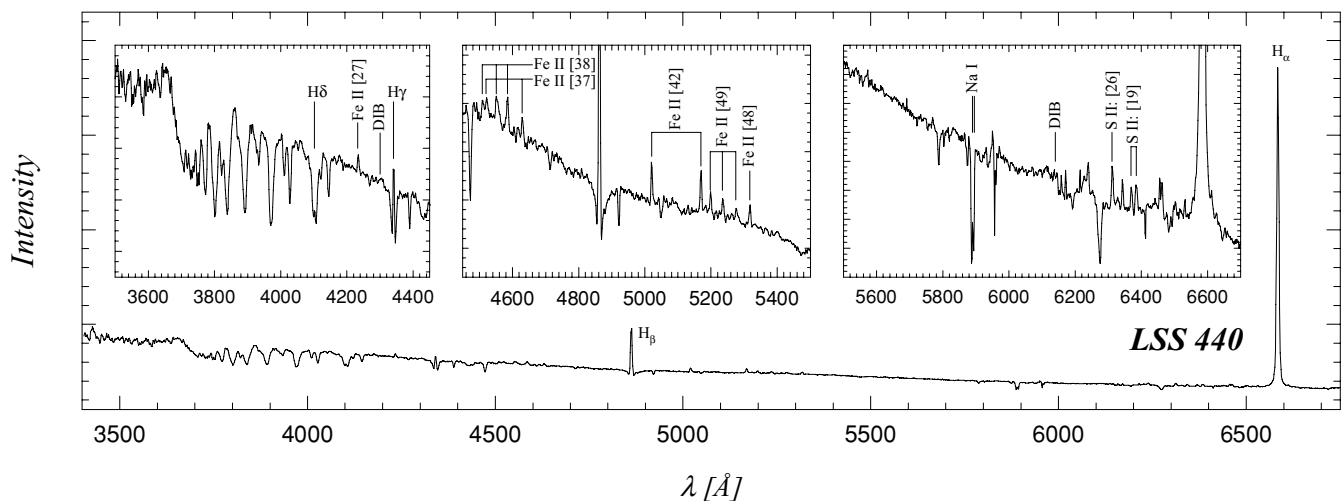


Figure 10. Complete observed spectrum of the LSS 440 star on the main panel and its main features in detail on the three upper minor panels.

of solar metallicity, a star with such properties should have a mass near $15 M_{\odot}$ and an age about $5-6 \times 10^6$ yr.

Likewise, based on the slope change of the star spectra from 4000 to 4600 Å and using the Chalonge & Divan (1973) calibration improvements to the BCD method by Cidale et al. (2001), we can compute the star visual absorption (A_V) produced by both the interstellar dust and the circumstellar envelope. The computations yielded $A_V = 1.33$, setting the true distance modulus of LSS 440 in $V_0 - M_V = 14.44 \pm 0.5$ corresponding to a distance $d = 7.7$ kpc.

Fabregat & Torrejón (2000) studied the abundance of Be stars in open clusters as a function of the cluster ages. Following these authors findings, Be-type stars show a maximum of appearance in clusters the age of NGC 2401. From this point of view, to find a Be-type star in this cluster should not be odd. However, the distance of LSS 440 disagrees with the cluster distance and it is placed a bit far from the cluster centre. Likewise, the mass of LSS 440 is extremely high if compared with the mass of next bright member star on the cluster MS (see Sections 3.3 and 5 in advance), which is ≈ 2 mag fainter. Certainly, the location of LSS 440 on the M_V versus $B - V$ and $U - B$ versus $B - V$ diagrams is in agreement with the usual location of other Be stars in open clusters (see figs 6a

and 7 given by Mermilliod 1982) but the available elements at the moment preclude any kind of clear physical relationship between the cluster and this star. Radial velocities would be a very useful tool to settle this question.

5 CLUSTER LUMINOSITY AND INITIAL MASS FUNCTIONS

For the construction of the cluster LF, defined as the distribution of stars over the magnitude range in bins 1 mag wide, we applied the procedure already described in Baume et al. (2004). That is, we first computed the apparent magnitude distribution of lm and pm stars for $V < 17$ (the LSS 440 star was not included in this analysis) and from the subtraction method for $V \geq 17$.

The latter procedure consists in a ‘cleaning’ of the CMD of all stars inside the cluster limits by removing the contribution of field stars projected onto the cluster itself. We assume that our CF provides a good estimation of the contamination by field interlopers and is valid across the ‘cluster area’. We tried to reduce the contamination coming from the Galactic disc population by means of two envelope curves around the MS on the V versus $V - I$ plane

Table 2. Stellar counts, completeness values and apparent cluster LF.

ΔV	Cluster area	Comparison field	Completeness (per cent)	Apparent LF
14–15	8	2	100.0	6
15–16	20	7	100.0	10
16–17	38	11	99.8	18
17–18	55	42	97.3	15
18–19	94	59	96.2	36
19–20	106	69	95.5	39
20–21	99	85	94.2	15
21–22	110	98	91.8	13
22–23	125	99	78.4	33
23–24	46	19	57.3	47

(dashed curves on Figs 6e and f). We located them reasonably far from the MS in order to include all cluster stars. Then, we used a separation from the MS of about 0.3 mag in colour for a given V magnitude, a value that was increased to faint magnitudes according to photometric errors. It is to be mentioned that the completeness of our data has been estimated as in Baume et al. (2004) and, like in that case, incompleteness is only severe at very faint magnitudes ($V > 21$).

Once the entire distribution of apparent magnitudes is ready, it is transformed into the M_V distribution using the cluster distance modulus of Section 3.3. The results are presented in Table 2 in a self-explanatory format.

Regarding the IMF, which is defined as the distribution of original ZAMS stellar masses in logarithmic bins, absolute magnitude intervals of the LF were converted into mass intervals using the mass–luminosity relation given by Scalo (1986). What we obtained is indeed the present day mass function (PDMF), which, in the case of NGC 2401, is very close to the IMF because only stars below the ‘turn-off’ are considered. The results shown in Fig. 11 indicate that the IMF displays a constant slope for the most massive bins (filled circles), while a small dip appears at about $2 M_\odot$ followed by another one, more noticeable, near $0.8 M_\odot$. Because the last (less massive) mass points (open circles) are dubious because of probable incompleteness, the dip could be an artefact; if not, they are suggesting a pronounced flattening of the mass function. The mass points of the most massive stars were fitted through a weighted least-squares

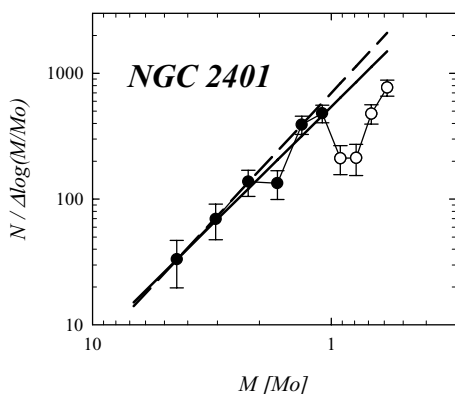


Figure 11. Initial mass function (IMF) of NGC 2401. Error bars are from Poisson statistics. The weighted least-squares fittings for the more massive bins are indicated by solid and dashed straight lines (open symbols indicate bins not used in the fits; see Section 5 for details).

fit that yielded a slope $x = 2.0 \pm 0.1$ for $M > 2 M_\odot$ and $x = 1.8 \pm 0.2$ for $M > 1 M_\odot$ (see Fig. 11).

6 A PROBABLE PMS STAR POPULATION IN NGC 2401

No doubt NGC 2401 is young and could still show hints of a PMS star population which is normally placed over the fainter part of the cluster above the MS. In fact, Figs 6(d) and (e) suggest the presence of a ‘turn-on’ point at $V \sim 17$ –18; however, the detection of a PMS star population at this magnitude level is hard due to the field contamination. Figs 6(a) and (b), on the other hand, are not deep enough to perform a trustable analysis of this type.

In order to clarify this point, we applied again the subtraction procedure using Figs 6(e) and (f) (see Section 5), but now selecting also stars by $V - I$ bins 0.25 mag wide (see Baume et al. 2003). This way, we could build an array indicating the amount of stars in each V and $V - I$ box, both for the ‘cluster area’ and for the CF. Then, by performing the difference between these two arrays, we notice an excess of stars present approximately in the path indicated by the long-dashed straight lines on Fig. 6(e). Therefore, this fact reinforces the probable existence of a PMS star population in NGC 2401. However, deeper photometric observations and/or spectroscopy of selected stars in this region would be important to confirm this issue.

7 NGC 2401 AND THE GALACTIC STRUCTURE IN THE THIRD GALACTIC QUADRANT

The distance and age of NGC 2401 (see Section 3.3) indicate this object belongs to the innermost side young population of the probable extension of the Norma–Cygnus spiral arm in the Third Galactic Quadrant. This outer spiral structure was already suggested by Vogt (1976) using Luminous Stars and, more recently, by Kalcheva & Hildilch (2000) studying OB stars. Star forming regions were found by Russeil (2003), though an inspection of his fig. 5 shows few young objects at the Galactic position of NGC 2401. The Georgelin & Georgelin (1976) list shows just one $H\alpha$ source, S 298, at a distance of 5.2 kpc but with a Galactic longitude of $227^\circ.7$. Also, few open clusters with ages less than 100 Myr are found in this region when inspecting the Dias et al. (2002) catalogue. It is obvious that the Norma–Cygnus arm can be optically detectable partially through windows in the interstellar absorption. However, May, Alvarez & Bronfman (2005) could trace this spiral arm by means of CO clouds and optical evidences of its existence have also been recently reported by Carraro et al. (2005b) who detected the presence of a large population of blue distant stars behind several open clusters in this Galactic Quadrant. In this sense, the cluster upper MS (see Fig. 6) of NGC 2401 coincides with the ‘blue plume’ seen in the cluster sample analysed by Carraro et al. (2005b), which they associate with a young population defining the Norma–Cygnus spiral arm. In fact, the brightest stars of NGC 2401 appear at $V \approx 14$ –15 and $B - V \approx 0.1$ and merge with old disc population at $V \approx 18$ just as stars in the ‘blue plume’ of Carraro et al. (2005b) do. So, NGC 2401 is then part of the small sample of very young open clusters presently known to trace the Norma–Cygnus arm: Bochum 2, Haffner 18, Dolidze 25 and Pismis 1, among others. The spatial distribution of CO clouds (May et al. 2005), the young distant population (Carraro et al. 2005b) and the distance of NGC 2401 suggest altogether it is located in the innermost side of the Norma–Cygnus arm. Therefore, NGC 2401 CMDs can be used in the future as a

possible template to recognize and match features such as the mentioned ‘blue plume’ seen in the optical CMDs of other places in the Third Galactic Quadrant.

We also have shown arguments that weaken the probable relationship of LSS 440 with NGC 2401: LSS 440 is placed at a distance $d = 7.7$ kpc, but the error in its M_V estimate and in the cluster distance modulus may locate the star as far from the Sun as 9.5 kpc or as close to it as 6.1 kpc. Only in this late marginal case, some relation can be stated, but we have already shown other arguments such as the star mass against that. By ignoring any connection between the cluster and the star, it becomes evident that unlike NGC 2401, LSS 440 is located well inside the Norma–Cygnus spiral arm so that, in any case, we are dealing with very young and remote objects that reinforce the spiral structure of the Milky Way in this quadrant of the Galaxy.

8 CONCLUSIONS

We have presented a detailed multicolour photometric study in the region of the open cluster NGC 2401, we confirmed the emission nature of LSS 440 and gave its first spectral type classification. In our opinion, the present state of knowledge of this star precludes discarding its membership to the cluster but no firm argument favouring its cluster membership has been found. NGC 2401 is a very young object (~ 25 Myr) placed at 6.3 ± 0.5 kpc from the Sun, which makes it an object located in the outskirts of our Galaxy and therefore a good tracer of the continuation of the Norma–Cygnus arm into the Third Galactic Quadrant. Not confirmed at all, we found weak evidences of a probable PMS star population accompanying this cluster. As for the cluster IMF, the slope value found for NGC 2401 is not far from the typical values shown by Scalo (1998, 2005).

ACKNOWLEDGMENTS

The authors thank the CASLEO staff for technical support and thank L. Cidale for very useful discussions and valuable comments. AM is grateful for the financial support from FCT (Portugal) grants BPD/20193/99, SFRH/BPD/19105/2004 and the YALO project (PESO/P/PRO/1128/96). GB acknowledges a postdoctoral grant from Padova University where part of this work has been performed. The work of GC has been partially supported by Fundación Andes. This research has been also carried out under the cooperative international agreement Argentino–Italiano SECYT-MAE (IT/PA03–UIII/077). The authors are much obliged for the use of the NASA Astrophysics Data System, of the SIMBAD data base (Centre de Donnés Stellaires – Strasbourg, France) and of the WEBDA open cluster data base. This publication also made use of data from the 2MASS, which is a joint project of the University of Massachusetts and the Infrared Processing and Analysis Center/California Institute of Technology, funded by NASA and the NSF.

REFERENCES

Barbier D., Chalonge D., 1941, *Ann. Astrophys.*, 4, 30
 Baume G., Vázquez R. A., Carraro G., Feinstein A., 2003, *A&A*, 402, 549
 Baume G., Moitinho A., Giorgi E. E., Carraro G., Vázquez R. A., 2004, *A&A*, 417, 961
 Carraro G., Munari U., 2004, *MNRAS*, 347, 625
 Carraro G., Geisler D., Baume G., Vázquez R. A., Moitinho A., 2005a, *MNRAS*, 360, 655
 Carraro G., Vázquez R. A., Moitinho A., Baume G., 2005b, *ApJ*, 630, L153
 Chalonge D., Divan L., 1952, *Ann. Astrophys.*, 15, 201

Chalonge D., Divan L., 1973, *A&A*, 23, 69
 Cidale L., Zorec J., Tringaniello L., 2001, *A&A*, 368, 160
 Cousins A. W. J., 1978a, *Mon. Notes Astron. Soc. S. Afr.*, 37, 62
 Cousins A. W. J., 1978b, *Mon. Notes Astron. Soc. S. Afr.*, 37, 77
 Dean J. F., Warren P. R., Cousins A. W. J., 1978, *MNRAS*, 183, 569
 Dias W. S., Alessi B. S., Moitinho A., Lépine J. R. D., 2002, *A&A*, 389, 871
 Fabregat J., Torrejón J. M., 2000, *A&A*, 357, 451
 Georgelin Y. M., Georgelin Y. P., 1976, *A&A*, 49, 57
 Giorgi E. E., Vázquez R. A., Baume G., Seggewiss W., Will J.-M., 2002, *A&A*, 381, 884
 Giorgi E. E., Baume G., Solivella S., Vázquez R. A., 2005, *A&A*, 432, 491
 Girardi L., Bressan A., Bertelli G., Chiosi C., 2000, *A&AS*, 141, 371
 Høg E. et al., 2000, *A&A*, 357, 367
 Jaschek M., Jaschek C., Hubert-Delplace A.-M., Hubert H., 1980, *A&AS*, 42, 103
 Kaltcheva N. T., Hildilch R. W., 2000, *MNRAS*, 312, 753
 Koornneef J., 1983, *A&A*, 128, 84
 Lyngå G., 1987, *Catalog of Open Star Cluster Data*. Centre de Donnés astronomiques de Strasbourg (CDS), Strasbourg
 Martin N. F., Ibata R. A., Bellazzini M., Irwin M. J., Lewis G. F., Dehnen W., 2004, *MNRAS*, 348, 12
 May J., Alvarez H., Bronfman L., 2008, submitted
 Mermilliod J.-C., 1982, *A&A*, 109, 48
 Meynet G., Mermilliod J.-C., Maeder A., 1993, *A&AS*, 98, 477
 Moitinho A., 2001, *A&A*, 370, 436
 Moitinho A., 2002, in Grebel E. K., Brandner W., eds, *ASP Conf. Ser. Vol. 285, Modes of Star Formation and the Origin of Field Populations*. Astron. Soc. Pac., San Francisco, p. 256
 Moitinho A., Alfaro E. J., Yun J. L., Phelps R. L., 1997, *AJ*, 113, 1359
 Moitinho A., Carraro G., Baume G., Vázquez R. A., 2006, *A&A*, 445, 493
 Momany Y., Zaggia S. R., Bonifacio P., Piotto G., DeAngeli F., Bedin L. R., Carraro G., 2004, *A&A*, 421, L29
 Russeil D., 2003, *A&A*, 397, 133
 Scalo J., 1986, *Fundam. Cosmic Phys.*, 11, 1
 Scalo J., 1998, in Gilmore G., Howell D., eds, *ASP Conf. Ser. Vol. 142, The Stellar Initial Mass Function*. Astron. Soc. Pac., San Francisco, p. 201
 Scalo J., 2005, in Corbelli E., Palla F., Zinnecker H., eds, *IMF@50: The Initial Mass Function 50 yr Later*. Kluwer, Dordrecht, in press (astro-ph/0412543)
 Schmidt-Kaler Th., 1982, in Schaifers K., Voigt H. H., eds, *Landolt-Börnstein, Numerical data and Functional Relationships in Science and Technology, New Series, Group VI, Vol. 2(b)*. Springer Verlag, Berlin, p. 14
 Stephenson C. B., Sanduleak N., 1971, *Publ. Warner & Swasey Obs.*, 1 (online reference: <http://vizier.cfa.harvard.edu/viz-bin/Cat?III/43>)
 Sujatha S., Babu G. S. D., Ananthamurphy S., 2004, *Bull. Astron. Soc. India*, 32, 295
 Vogt N., 1976, *A&A*, 53, 9
 Zacharias N., Urban S. E., Zacharias M. I., Wycoff G. L., Hall D. M., Monet D. G., Rafferty T. J., 2004, *AJ*, 127, 3043
 Zorec J., 1986, PhD thesis, Univ. Paris VII, Denis Diderot
 Zorec J., Fre’mat Y., Huber A. M., Floquet M., 2002, in Aerts C., Bedding T. R., Christensen-Dalsgaard J., eds, *ASP Conf. Ser. Vol. 259, IAU Colloq. 185, Radial and Nonradial Pulsations as Probes of Stellar Physics*. Astron. Soc. Pac., San Francisco, p. 244

SUPPLEMENTARY MATERIAL

The following supplementary material is available for this article online (at <http://www.blackwell-synergy.com/>):

Table 1. Photometric catalogue of the NGC 2401 region.

This paper has been typeset from a $\text{\TeX}/\text{\LaTeX}$ file prepared by the author.